A99-31068

AIAA 99–2209

On LEM/LES Methodology for Two-Phase Flows

S. Pannala and S. Menon
School of Aerospace Engineering
Georgia Institute of Technology
Atlanta, Georgia 30332-0150

35th AIAA/ASME/SAE/ASEE Joint Propulsion Conference and Exhibit
June 20-23, 1999 / Los Angeles, California

On LEM/LES Methodology for Two-Phase Flows*

S. Pannala† and S. Menon‡
School of Aerospace Engineering
Georgia Institute of Technology
Atlanta, GA 30332-0150

ABSTRACT

A two-phase subgrid combustion model developed earlier has been evaluated for applicability in large-eddy simulations (LES). Direct Numerical Simulations (DNS) of two-phase isotropic turbulence in the presence of passive, momentum-coupled and vaporizing droplets has been extensively studied to form a base-line database. Current DNS results agree with earlier studies and show that the presence of droplets increase the kinetic energy and dissipation at the small scales. LES for these same cases were also carried out to investigate what modifications are needed to incorporate the small-scale turbulence modifications seen in DNS of two-phase flows. LES subgrid modeling for two-phase mixing within the context of the new subgrid combustion model is also addressed.

INTRODUCTION

Liquid fuel is used in many of the conventional engines (e.g., gas-turbine, internal combustion and diesel engines). Environmental concerns, government regulations and commercial viability makes it imperative to increase efficiency and reduce emissions. To achieve these desired features, there is a need to develop numerical methods which can accurately capture liquid fuel atomization process and fuel-air mixing downstream of the fuel injector. Steady-state methods are not suitable for studying highly unsteady fuel atomization and fuel-air mixing processes. On the other hand, although the unsteady mixing process can be studied quite accurately using direct numerical simulation (DNS) (e.g., Poinsot, 1996), the application of DNS is limited to low to moderate Reynolds numbers (Re) due to resolution requirements and therefore, cannot be used for high Re flows of current interest.

LES seems to be a viable approach to model combustion (Kim and Menon, 1999) and two-phase flows (Pannala and Menon, 1998; Menon et. al, 1999). In LES, the scales larger than the grid are computed using a time- and space-accurate scheme, while the unresolved smaller scales are modeled. Closure of momentum and energy transport equations can be achieved using a subgrid eddy viscosity model since the small scales primarily provide a dissipative mechanism for the energy transferred from the large scales. However, for combustion to occur, the species must first undergo mixing and come into molecular contact. These processes occur at the small scales which are not resolved in the conventional LES approach. As a result, conventional subgrid eddy diffusivity models cannot capture all these features.

To address these issues a subgrid combustion model was developed and implemented within the LES formulation (Menon et al., 1993; Menon and Calhoon, 1996; Calhoon and Menon, 1996, 1997). This model separately and simultaneously treats the physical processes of molecular diffusion and small scale turbulent convective stirring. This is in contrast to probability density function closure where molecular diffusion processes are to be modeled, thereby making it difficult to address experimentally observed Schmidt number variations of the flow.

The gas-phase methodology was recently extended to two-phase flows (Menon and Pannala, 1997 and Pannala and Menon, 1998) to accurately capture the process of phase change and turbulent mixing. In the present paper, this approach has been revisited using forced isotropic turbulence.

Of particular interest for LES of two-phase flows is the proper characterization of the effects of turbulence on droplet properties as well as the reverse effect of droplet drag and vaporization on turbulence. The past

†. Currently at Oak Ridge National Labs, Oak Ridge, TN.
‡. Professor, Senior Member, AIAA

LES studies of Oefelein and Yang (1996) included the effect of turbulence on droplet characteristics but the modulation of the turbulence by the droplets was ignored. However, several studies (e.g. recent ones by Mashayek, 1998; Boivin et al., 1998) have shown that droplet drag and vaporization can have significant effect on turbulence. These studies as well as the earlier ones (Elgobashi and Truesdell, 1991, 1993 & 1994; Squires and Eaton, 1990 & 1991) demonstrated that depending upon the mass loading and droplet sizes, the droplets can change the energy transfer process leading to an increase in the turbulent kinetic energy at the small scales. Associated with this increase is an increase in the energy dissipation at the small scales. Since the small scales are not resolved in a LES it is of interest to determine what features of the small-scale effect caused by droplet-turbulence interactions need to be included in the subgrid model.

In order to address this problem, several DNS of forced isotropic turbulence were carried out to characterize the effects of momentum-coupled and vaporizing sprays on gas-phase flows. The results were then analyzed using energy and dissipation spectra, Lagrangian correlations (both particle-particle and fluid-particle) and other statistical quantities. Finally, LES were conducted with and without the new subgrid mixing model to evaluate its ability to deal with small-scale droplet-turbulence interactions.

FORMULATION

Both Eulerian and Lagrangian formulations have been used to simulate two-phase flows in the past (e.g., Mostafa and Mongia, 1983). However, most state-of-the-art codes employ the Lagrangian form to capture the droplet dynamics, while the gas phase is computed in the Eulerian form (e.g., Oefelein and Yang, 1996). In this formulation, the droplets are tracked explicitly using Lagrangian equations of motion, and heat and mass transfer are computed for each droplet. Due to resource constraints (computer time and memory), only a limited range of droplet sizes are computed. Droplets below an *ad hoc* cut-off size are assumed to vaporize instantaneously and to become fully mixed in the gas phase. This is a flawed assumption, since even in pure gas flows small-scale mixing process is very important for quantitative predictions (Menon and Calhoon, 1996). Here, the gas-phase subgrid combustion methodology has been extended to allow proper simulation of the final stages of droplet evaporation and turbulent mixing.

The two-phase subgrid process is implemented within the framework of the Eulerian-Lagrangian LES approach. Thus, droplets larger than the cut-off size are tracked as in the usual Lagrangian approach. However, once the droplets are smaller than the cut-off, a two-phase subgrid Eulerian model is employed to include the effects of the small droplets within the LES cells.

Gas Phase LES Equations

The incompressible Navier Stokes equations in the zero Mach number limit are employed for the present study. Zero-Mach number approach involves using a series expansion in terms of Mach number to remove the acoustic component from the equations and is a well established method (McMurtry et al., 1989; Chakravarthy and Menon, 1997).

The LES mass, momentum, energy and species equations in the zero-Mach number limit are:

$$\frac{\partial \rho}{\partial t} + \frac{\partial \rho \bar{u}_i}{\partial x_i} = \dot{\rho}_s \tag{1}$$

$$\frac{\partial \rho \bar{u}_i}{\partial t} + \bar{u}_j \frac{\partial \rho \bar{u}_i}{\partial x_j} = \frac{\partial \bar{p}}{\partial x_i} + \mu \frac{\partial^2 \bar{u}_i}{\partial x_k \delta x_k} + \frac{\partial \tau_{ij}}{\partial x_j} + \dot{F}_{s,i} \tag{2}$$

$$\frac{\partial \bar{u}_i}{\partial x_i} = \frac{\Upsilon - 1}{\Upsilon} \frac{1}{\hat{p}} \Big[\lambda \frac{\partial^2 T}{\partial x_k \partial x_k} - \frac{\Upsilon}{\Upsilon - 1} \frac{\partial \hat{p}}{\partial t} + \dot{Q}_s - \dot{F}_{s,i} + \dot{\rho}_s ((\bar{u}_i \bar{u}_i)/2) \Big] \tag{3}$$

$$\frac{\partial \rho \overline{Y_\alpha}}{\partial t} + \frac{\partial \rho \overline{Y_\alpha} u_j}{\partial x_j} = D \frac{\partial^2 \overline{Y_\alpha}}{\partial x_k \partial x_k} + \frac{\partial S_{\alpha j}}{\partial x_j} + \overline{\dot{\omega}_\alpha} + S_{s,\alpha} \tag{4}$$

The above system of equations is supplemented by the equation of state for the thermodynamic pressure $\hat{p} = \rho R T$ which can be used to obtain the temperature T. Here, ρ, $\bar{u}_i$, $\overline{Y_\alpha}$ and $\bar{p}$ are, respectively, the density, i-th velocity component, α-th species mass fraction and the kinematic pressure. Also, ν, λ, D and R are, respectively, the kinematic viscosity, the thermal conductivity, the mass diffusion (assumed constant and same for all species here, but can be generalized) and the gas constant. In Eq. (4), $\overline{\dot{\omega}_\alpha}$ is the LES filtered species production/destruction term. Also, in the above equations, source terms $\dot{\rho}_s, \dot{F}_s, \dot{Q}_s$, and S_s represent the volume-averaged rate of exchange of mass, momentum, energy and species between the gas-phase and the liquid phase. These terms are computed, as detailed elsewhere (Oefelein and Yang, 1996; Faeth, 1983) and, therefore, omitted here for brevity.

Furthermore, note that Eq. (3) is the equivalent energy equation in the zero-Mach number limit. In the absence of heat release and no phase change, this equation and Eq. (1) will be identical.

In the above equations, the subgrid stress tensor $\tau_{ij} = -(\overline{u_i u_j} - \bar{u}_i \bar{u}_j)$ and the species-velocity correlations $S_{\alpha j} = -(\overline{Y_\alpha u_j} - \overline{Y}_\alpha \bar{u}_j)$ require modeling. In the present LES approach, the stress term τ_{ij} is modeled as $\tau_{ij} = 2\nu_t S_{ij}$ where ν_t is the eddy viscosity and S_{ij} is the resolved rate-of-strain tensor. The subgrid eddy viscosity is obtained in terms of the grid scale Δ and the subgrid kinetic energy, $k^{sgs} = (\overline{u_i u_i} - \bar{u}_i \bar{u}_i)$ as: $\nu_t = C_\nu \sqrt{k^{sgs}}\Delta$. Here, k^{sgs} is obtained by solving a transport equation and is described in next section.

Liquid-phase LES equations

A Stochastic Separated Flow (SSF) formulation (Faeth, 1983; Oefelein and Yang, 1996) is used to track the droplets using Lagrangian equations of motion. The general equations of spherical droplets reduce to the following form (here, terms arising due to static pressure gradient, virtual-mass, Basset force and external body-forces are neglected for simplicity):

$$\frac{dx_{p,i}}{dt} = u_i \tag{5}$$

$$\frac{du_{p,i}}{dt} = \frac{3}{4} C_D Re_p \frac{\mu}{\rho_p d_p^2}(u_i - u_{p,i}) \tag{6}$$

where the droplet properties are denoted by subscript p, d_p is the droplet diameter and u_i is the instantaneous gas phase velocities computed at the droplet location. This gas phase velocity field is obtained using both the filtered LES velocity field $\bar{u}_i$ and the subgrid kinetic energy k^{sgs} (as in the eddy interaction model). The droplet Reynolds number is computed using: $Re_p = \frac{d_p}{\nu}[(u_i - u_{p,i})(u_i - u_{p,i})]^{1/2}$ and the drag coefficient is modeled by (Faeth, 1983):

$$C_D = \begin{cases} \frac{24}{Re_p}\left(1 + \frac{1}{6}Re_p\right) & Re_p \le 10^3 \\ 0.424 & Re_p > 10^3 \end{cases} \tag{7}$$

The conservation of the mass of the droplets results is given by: $d\dot{m}_p/dt = -\dot{m}_p$ where the mass transfer rate for a droplet in a convective flow field is given as:

$$\frac{\dot{m}_p}{\dot{m}_{Re_p=0}} = 1 + \frac{0.278 Re_p^{1/2} Sc^{1/3}}{[1 + 1.232/Re_p Sc^{2/3}]^{1/2}} \tag{8}$$

Here, Sc is the Schmidt number and the subscript $Re_p = 0$ indicates quiescent atmosphere when there is no velocity difference between the gas and the liquid phase. The mass transfer under this condition is given as $\dot{m}_{Re_p=0} = 2\pi\rho_s D_{sm} d_p ln(1 + B_M)$. Here, ρ_s and D_{sm} are, respectively, the gas mixture density and the mixture diffusion coefficient at the droplet surface and B_M is the Spalding number which is given as $B_M = (Y_{s,F} - Y_{\infty,F})/(1 - Y_{s,F})$. Here, $Y_{s,F}$ is the fuel mass fraction at the surface of the droplet and computed using the procedure described in Chen and Shuen (1993), while $Y_{\infty,F}$ is the fuel mass fraction in the ambient gas.

The heat transfer rate of the droplet (assuming uniform temperature in the droplet) is given by the following relation (Faeth, 1983):

$$m_p C_{p,p} \frac{dT_p}{dt} = h_p \pi d_p^2 (T - T_p) - \dot{m}_p \Delta h_v \tag{9}$$

The heat transfer coefficient for a droplet in a convective flow field with mass transfer is modeled as

$$\frac{h_p}{h_{Re_p=0}} = 1 + \frac{0.278 Re_p^{1/2} Pr^{1/3}}{[1 + 1.232/Re_p Pr^{2/3}]^{1/2}} \tag{10}$$

Here, Pr is the gas phase Prandtl number and the heat transfer coefficient for quiescent medium is given as $h_{Re_p=0} = \lambda Nu_{Re_p=0}/d_p$ where the Nusselt number is obtained from:

$$Nu_{Re_p=0} = \frac{2 ln(1 + B_M)^{Le^{-1}}}{(1 + B_M)^{Le^{-1}} - 1} \tag{11}$$

$Nu_{Re_p=0}$ approaches a value of 2 in the case of zero mass transfer and Le is the Lewis number. Only droplets above a cut-off diameter are solved using the above equations, while the droplets below the cut-off diameter are modeled using Eulerian formulation within the subgrid.

In summary, the present LES approach solves only the momentum equations on the LES grid. Closure for the subgrid stresses is achieved by using a localized dynamic model for the subgrid kinetic energy. Concurrently, the liquid phase equations are solved using the Lagrangian technique. The range of droplet sizes tracked depends on the computational constraints. The gas phase LES velocity field and the subgrid kinetic energy are used to estimate the instantaneous gas velocity at the droplet location. This essentially provides a coupling between the gas and liquid phase momentum transport. The mass conservation and the gas phase scalar field equations are simulated in the subgrid domain as discussed in the next section.

SUBGRID MODELS

Closure of the above LES equations (both gas and liquid phases) require models for the unresolved terms. Two types of closure are needed: a closure for momentum transport and a closure for the scalar transport (both gas and liquid phases). The closure for the momentum transport is achieved by using an eddy viscosity model which is considered reasonable since the small scales are assumed to primarily provide dissipation for the energy transferred from the large scales. The specification of the eddy viscosity requires a length and a velocity (or a time) scale. Many past LES studies have employed an algebraic eddy viscosity model which uses the grid size as the length scale and the resolved rate-of-strain tensor as the time scale. However, this model has some serious limitations. For example, this approach requires equilibrium between turbulent kinetic energy production and dissipation in the small scales which is possible only if a very high resolution LES grid is employed such that only the dissipation scales are unresolved. Such high resolution simulations are not feasible in practice due to resource constraints.

In the present study (as well as the earlier effort, Menon and Pannala, 1997), a subgrid model based on the subgrid kinetic energy is employed to obtain the characteristic velocity scale. With this approach, the equilibrium requirement can be relaxed and coarser grid LES is possible as demonstrated earlier (Kim and Menon, 1998). Furthermore, to model turbulent dispersion of particles the subgrid kinetic energy provides the required information which is absent in the algebraic model closure. In earlier LES studies by Wang and Squires (1996), subgrid kinetic energy equation was explicitly carried to provide additional information to supply velocity variations for the Lagrangian tracking scheme of the particles.

3.1 The Subgrid Momentum Closure

The subgrid closure of the unresolved stresses and energy flux is achieved in the present approach by solving a transport model for the subgrid kinetic energy, k^{sgs}. Details have been reported elsewhere. Here, the extension of the earlier model for gas phase to two-phase flows has been carried out. The final form is:

$$\frac{\partial \rho k^{sgs}}{\partial t} + \frac{\partial}{\partial x_i}(\rho \bar{u}_i k^{sgs}) = T_k + P_k - D_k + F_k \qquad (12)$$

Here, $T_k = \frac{\partial}{\partial x_i}\left(\frac{\nu_t}{\sigma_k}\frac{\partial k^{sgs}}{\partial x_i}\right)$ is the transport term and $\sigma_k \approx 1.$ is a constant. The other terms, P_k and D_k are respectively, production and dissipation of k^{sgs}. The last term F_k is unique to two-phase flows and represents the work done due to the two-phase coupling force term $\dot{F}_{s,i}$. This term (similar to terms in the LES equations, Eq. 2) provides the coupling between the turbulent motion of the droplets and the evolution of the subgrid kinetic energy. The closure of Eq. (12) is obtained using $P_k = -\tau_{ij}^{sgs} S_{ij}$, $D_k = C_\varepsilon \rho \frac{k^{sgs3/2}}{\Delta}$ and

$$F_k = \overline{\dot{F}_{s,i} u_i} - \overline{\dot{F}_{s,i}} \bar{u}_i \qquad (13)$$

Here, C_ε is another coefficient that must be obtained (along with C_ν) using the dynamic procedure.

The expression in Eq. (13) represents the direct effect of two-phase coupling on k^{sgs} and requires modeling. Note that, k^{sgs} is indirectly modified due to particle motion and vaporization since the force term $\dot{F}_{s,i}$ will change the resolved velocity field (via Eq. 2) which in turn will change the resolved subgrid kinetic energy. Inclusion of the term F_k allows for an additional (direct) modification of the subgrid kinetic energy due to interaction between the particles and the *unresolved* small scale motion. Here the term in Eq. (13) is modeled as follows:

$$F = \langle u_i \dot{F}_{s,i} \rangle - \bar{u}_i \langle \dot{F}_{s,i} \rangle \qquad (14)$$

Here, $\langle\ \rangle$ represents an average over all the droplet trajectories crossing the cell. This closure is very similar to that of Chen and Pereira (1998), where it has been applied in a k-ε Reynolds-averaged

formulation. Since all the necessary information for closure is available, this is complete representation and no tunable constants are required.

Thus, the presence of the droplets can have a two-fold effect. The first effect is directly on the LES resolved momentum transport due to the coupling force term, $\dot{F}_{s,i}$. The second effect is the modification to the subgrid kinetic energy due to the force term Eq. (14) which accounts for the interaction between the particles and the small-scale unresolved turbulent field.

3.2 The Subgrid Species Closure

The principle difficulty in reacting LES simulations is the proper modeling of the combustion related terms involving temperature and species, for example, the subgrid species fluxes and the filtered species mass production rate $\dot{\omega}_\alpha$. Probability density function methods when applied within LES either using an assumed shape or an evolution equation may be used to close $\dot{\omega}_\alpha$ and, in principle, any scalar correlations. However, the treatment of molecular mixing and small scale stirring using phenomenological models as in pdf methods, have not been very successful in predicting the mixing effects. Problems have also been noted when the gradient diffusion model is used to approximate the species transport terms.

The linear eddy mixing (LEM) model (Kerstein, 1989) treats separately molecular diffusion and turbulent mixing processes at all relevant length scales of the flow. The scalar fields are simulated within a 1D domain which, in the context of LES, represents a 1D slice of the subgrid flame brush. The subgrid model simulates only the effect of the small unresolved scales on the scalar fields while the larger resolved turbulent scales of the flow are simulated by the LES equations. The subgrid LEM has several advantages over conventional LES of reacting flows. In addition to providing an accurate treatment of the small-scale turbulent mixing and molecular diffusion processes, this method avoids gradient diffusion modeling of scalar transport. Thus, both co- and counter-gradient diffusion can be simulated. More details of this approach (which is identical to the method used for gas phase LES) are given elsewhere (Menon and Calhoon, 1996; Calhoon and Menon, 1996, 1997) and therefore, avoided here.

3.2.1 The Single Phase Model

In the baseline model the exact reaction-diffusion equations are numerically solved using a finite-difference scheme in the local subgrid 1D domain using a grid fine enough to resolve the Kolmogorov microscales. Consequently, the production rate $\dot{\omega}_\alpha$ can be specified in the subgrid without any modeling. Simultaneous to the deterministic evolution of the reaction-diffusion processes, turbulent convective stirring within the 1D domain is modeled by a stochastic mapping process (Kerstein, 1992). This procedure models the effect of turbulent eddies on the scalar fields and is implemented as an instantaneous rearrangement of the scalar fields without changing the magnitudes of the individual fluid elements, consistent with the concept of turbulent stirring.

The implementation of the stirring process requires (randomly) determining the eddy size l from a length scale pdf $f(l)$ in the range $\eta \le l \le l_{LEM}$ where η is the Kolmogorov scale and l_{LEM} is the characteristic subgrid length scale which is currently assumed to be the local grid resolution Δ. A key feature of this approach is that this range of scales is determined from inertial range scaling as in 3D turbulence for a given subgrid Reynolds number: $Re_{LEM} = u' l_{LEM}/\nu$ where, u' is obtained from k^{sgs}. Thus, the range of eddy sizes and the stirring frequency incorporates the fact that the small scales are 3D. This feature is one of the major reasons for the past successes of LEM in gas phase diffusion flame studies (Menon and Calhoon, 1996; Calhoon and Menon, 1996, 1997).

Modifications for two-phase flows need to be considered in this formulation. The stirring process uses inertial range scaling laws which do not account for the presence of droplets. Since droplet motion and vaporization can change the turbulent spectra in the inertial range then this information needs to be incorporated. The following modifications to $f(l)$ and the event frequency have been made to account for the effect of droplets on the turbulent field. If the inertial scaling law is p-3 (for the Kolmogorov spectra p would be 4/3), then the distribution $f(l)$ and event frequency parameter (λ) are given as (Kerstein, 1991):

$$f(l) = \frac{3-p}{l_{lem}[(l_{lem}/\eta)^{3-p}-1]}(l_{lem}/\eta)^{p-4} \qquad (15)$$

$$\lambda = \frac{27}{2}\frac{p}{3-p}\frac{D_T}{l^3_{lem}}\frac{(l_{lem}/\eta)^{3-p}-1}{1-(\eta/l_{lem})^p} \qquad (16)$$

The value of the exponent p needs to be determined for the case with droplets.

3.2.2 The Two-Phase Model

For two-phase flows, the LEM reaction-diffusion equations have been modified to include two new features: (a) the vaporization of the droplets tracked by the Lagrangian method, and (b) the vaporization of droplets below the cut-off so that the final stages of droplet vaporization and mixing are included. However, some changes are required since droplet vaporization will change the subgrid mass of the gas (primarily the fuel). Thus, in addition to the scalar reaction-diffusion equations, the two-phase mass conservation equations must be solved in the subgrid.

The droplets below the cutoff have been included by assuming that the droplets act as a psuedo-fluid and therefore, the overall effect of the droplets within each LES cell can be modeled as a void fraction. This approach is valid only when the droplets form only a small fraction of the total volume and are small. However, this is an acceptable assumption here since all droplets larger than the cut-off are still tracked using the Lagrangian approach. The present Eulerian two-phase approach is also preferred (in terms of accuracy) when compared to the Lagrangian approach when the droplets are very small and begin to behave more like a continuum fluid.

Mass conservation in both the phases in the LEM is given by: $\rho_g\varphi + \rho_l(1-\varphi) = \rho_{avg}$, where subscript g represents gas phase, l the liquid phase and φ is the volume fraction of the gas phase (1 - void fraction of the liquid (λ)). The void fraction λ or φ evolve during the subgrid evolution. Although, the liquid density is a constant, the gas density ρ_g changes and needs to be determined. The mass conservation of each phase is imposed in the subgrid scales and are obtained from the following equations:

$$\frac{\partial \rho_g \varphi}{\partial t} = S_L + S_2 \qquad (17)$$

$$\frac{\partial (1-\varphi)\rho_l}{\partial t} = S_1 - S_2 \qquad (18)$$

Here, the source term S_1 is the contribution of the supergrid droplets (i.e., the LES-resolved Lagrangian droplets) to the subgrid liquid phase when the droplet size falls below the cutoff. S_L is due to vaporization of the droplets tracked in the supergrid and S_2 represents vaporization of liquid in the subgrid.

The gas phase species equation for any scalar mass fraction (Ψ) in the subgrid can be written as

$$\frac{\partial \rho_g \varphi\psi}{\partial t} = D\frac{\partial^2(\rho_g\varphi\psi)}{\partial s^2} + \dot{\omega}_\psi + S_\psi + S_L \qquad (19)$$

Here, "s" indicates the 1D domain of LEM. Also, S_ψ is the source term (only in the fuel species equation) for production due to vaporization of the liquid phase. An equation for temperature must also be solved with the above equations since vaporization requires heat absorption and is followed by a drop in temperature. This is quite similar to the method used in the earlier gas phase studies of heat release effect (Calhoon and Menon, 1997).

Note that, in Eqs. (17-19) the convective terms are missing. This is consistent with the LEM approach, whereby, the convection of the scalar fields is modeled using two distinct and concurrent processes: the small-scale turbulent stirring which accounts for convection in the small scales and the splicing process which accounts for convection of scalars at the LES resolved scales. Some comments regarding the large-scale convection process is given in the next section.

3.3 Subgrid implementation

Since the filtered species $\bar{Y}_\alpha$ and the mixture density ρ are calculated directly by filtering the subgrid Y_α and ρ_{avg} fields, there is no need to solve the equivalent LES filtered mixture mass and species conservation equations (i.e., Eqs. 1 and 4). Consequently, use of conventional (gradient diffusion) models is avoided. However, since both Y_α and ρ_{avg} subgrid fields are also influenced by large scale convection (due to the velocity field $\tilde{u}_i$ and the subgrid turbulent fluctuation estimated from k^{sgs}), additional coupling processes are required.

The convection of the scalar fields by the LES field across LES cell faces is modeled by a "splicing" algorithm (Menon et al., 1993; Menon and Calhoon, 1996; Calhoon and Menon, 1996). Details of this process are given in the cited references. Given the initial subgrid scalar fields and void fraction, droplet vaporization, reaction-diffusion, turbulent stirring, and large scale convection processes are implemented as discrete events within each LES cell. The epochs of these processes are determined by their respective time scales.

The splicing algorithm transports subgrid fluid elements from one LES cell to another based on the

local velocity field. The local velocity consists of the resolved velocity $\bar{u}_i$ plus a fluctuating component (estimated from the subgrid kinetic energy). The splicing events are implemented discretely on the convective time scale. Each splicing event involves (1) the determination of volume transfer between adjacent LES grid cells, (2) the identification of the subgrid elements to be transferred, and (3) the actual transport of the identified fluid elements. The underlying rationale for this procedure has been discussed elsewhere (Menon et al., 1993; Calhoon and Menon, 1996). The same algorithm is used here.

An important property of the splicing algorithm is that the species convection is treated as in Lagrangian schemes. Thus, convection is independent of the magnitude or gradient of the species which are transported and depends only on the velocity field. This property allows this algorithm to avoid false diffusion associated with numerical approximation of convective terms in differential equations. By avoiding both numerical and gradient diffusion, the splicing algorithm allows an accurate picture of the small scale effects of molecular diffusion to be captured, including counter-gradient and differential diffusion effects.

RESULTS AND DISCUSSION

The two-phase subgrid model has been implemented into a zero-Mach number code. The code is a finite difference semi-implicit solver that is second-order accurate in time, and uses a fifth-order upwind biased stencil for the convective terms, a fourth-order central scheme for the viscous terms and a second-order scheme for the solution of the Poisson equation for pressure.

The Lagrangian tracking of the droplets is carried out using a fourth-order Runge-Kutta scheme and the gas phase properties at the droplet location are obtained using a fourth order Lagrangian interpolation scheme. The droplet source terms are projected onto the surrounding gas-phase nodes. Two methods were investigated for this interpolation. In first case, all the weights were assumed to be the same and in the second case, they were calculate based on the droplet distance to the nodes. Both cases gave statistically similar results and thus, the equal-weights method was used in these simulations.

The simulations were started from a stationary state of 64^3 pseudo-spectral simulation of isotropic turbulence (Yeung and Pope, 1989). The simulations were forced using an integrated stochastic forcing scheme with the same parameters as those used by Yeung and Pope (1989). The forcing accelerations are calculated in the spectral space as in the pseudo-spectral codes, transformed to the physical space and then added to the velocities. The forcing for the LES cases is also carried out at the 128^3 resolution and filtered down to 64^3 to preserve similarity and to remove uncertainty. The simulations were time advanced for several flow-through times till a statistically stationary state evolved. Statistics were collected over 15 eddy-turn over times for validation.

For the two-phase DNS, droplets were added to this field so that the initial flow field is statistically homogeneous. The two-phase DNS evolved in time for 3-4 eddy-turn over times before statistics were collected for another 3-4 eddy-turn over times.

DNS of single-phase forced isotropic turbulence

Validation of the baseline code was carried out by carrying out DNS of forced isotropic turbulence using the method noted above. Stochastically forced turbulence at a $Re_\lambda \sim 62$ was simulated using a 128^3 grid. Normalized energy spectra and dissipation spectra are compared to the experiments (Re_λ=65) of Comte-Bellot & Corrsin (1971) and the DNS (Re_λ=63) of Yeung and Pope (1989). Good agreement with experiments and earlier simulations at high wavenumbers is evident from Figure 1a for both the energy and dissipation spectra.

Figure 1b shows the Kolmogorov scaled kinetic energy spectra. Also shown are lines corresponding to values of 1.5 and 2.5 on y-axis. At the Reynolds-number simulated one expects a small inertial region and the plateau gives the value of the Kolmogorov constant close to 2. This is close to the value computed in earlier DNS (Yeung, 1996) and near the experimentally observed value of 1.5.

Yeung and Pope (1989) use $k_{max}\eta$ to characterize the resolution of the simulations (k_{max} is the maximum wavenumber). In pseudo-spectral codes this has to be > 1.5 for adequate resolution. The resolution for the current DNS is also adequate with $k_{max}\eta \sim 2.3$. To further verify this, the dissipation skewness (S_ε) defined as (Kerr, 1985):

$$S_\varepsilon = \frac{4}{35}\left(\frac{15\nu}{\langle\varepsilon\rangle}\right)^{\frac{3}{2}} \int_0^{k_{max}} \nu k^4 E(k)\,dk \qquad (20)$$

was computed. Here, E(k) is the energy spectrum function at the scalar wavenumber $k \equiv (\underline{k}\cdot\underline{k})^{1/2}$, ν is the kinematic viscosity and $\langle\varepsilon\rangle$ is the volume-averaged

dissipation obtained by integrating the dissipation spectrum D(k), defined by $2\nu k^2 E(k)$. We obtained a value of 0.53 which is very close to the asymptotic value of 0.5 for high-Re. This also compares very well to the values reported by Eswaran and Pope (1988) and Yeung and Pope (1989).

Analysis of other statistical parameters confirmed that the present physical space code is capable of accurately simulating this flow field. Therefore, we can now use this code to study other relevant issues.

Momentum-coupled two-phase isotropic turbulence

To study two-way coupling (due to the source term in the momentum equation 2) between the gas-phase and the liquid-phase simulations were carried out with 32^3 stochastic droplets. The actual number of particles is dictated by the mass-loading (ϕ), density of the particle (ρ_p) and droplet diameter (d_p). The statistical error (which varies as $1/(\sqrt{N})$) is less than 1% for the current number of droplets.

Figure 2a shows the effect of droplets on normalized energy spectrum. As observed in earlier studies (e.g. Squires and Eaton, 1990) there has been an increase in energy at the high wavenumbers (small scales). However, this increase depends upon the mass loading and the present result agrees very well with past observations that energy increase at the small scales occurs more with higher mass loading. Figure 2b shows the corresponding dissipation spectrum. Since there is more energy at the small scales, there is also more dissipation (note $D(k) = 2\nu k^2 E(k)$).

The primary effects of the droplets are (i) to rearrange the energy in the wavenumber space and (ii) to dissipate energy. This is evident in Figure 3a, where the equilibrium values of the kinetic energy ($1/2q^2$) and mean dissipation ($\langle\varepsilon\rangle$) are plotted for various mass loadings. The values are normalized by the respective quantities for the no-coupling case. It is very evident that kinetic energy of the system decreases because of the dissipation by the droplets. The equilibrium values are thus lower than the corresponding non-coupled case and decrease with increased mass loading. These results are in good agreement with those of Boivin et al. (1998) and Squires and Eaton (1990).

The dissipation skewness, described earlier is plotted for various mass loadings in fig. 3b. This higher-order, small-scale parameter increases with increase in mass-loading. This reflects the increase in dissipation at the high wavenumbers and the increased activity at the small-scales. Analysis of transfer spectra (e.g. Boivin et. al., 1998) can be used to determine the energy transfer across the wavenumbers and subsequent dissipation mechanism. This study is underway.

One of the parameters which characterizes the particle response is the particle Stokes Number (St) defined as $St = \tau_p/\tau_e$. Here, τ_p is the particle response time given by $\rho_p d_p^{\,2}/18\mu$ and τ_e is the eddy turn over time calculated using integral length scale and u'. For low mass loading case (ϕ=0.1) and for small particles (St < 0.4) figs. 4a and 4b shows that there is negligible effect on the energy and dissipation spectra.

Droplets with St ~ 1 under the experience of centrifugal forces accumulate in the regions of low vorticity. This feature has been observed in isotropic turbulence (e.g. Squires and Eaton, 1990) and in forced shear layers (e.g. Lazaro and Lasheras, 1992; Martin and Meiburg, 1994; Pannala and Menon, 1998; Menon and Pannala, 1998). The same phenomena can be observed here by comparing figs. 5a and 5b.

These results suggest that the present DNS study has been able to capture all the essential features of two-way momentum coupling observed in past. This forms the basis for studying the effect of vaporizing droplets and is covered in the next sub-section.

Vaporizing droplets in isotropic turbulence

Vaporization is turned on from an initial equilibrium solution of forced isotropic turbulence with suspended particles. Since this is a time evolving process and there is continual addition of mass, and exchange of momentum and energy (kinetic and thermal), even with forcing no stationary state can be reached. Furthermore, in a periodic domain high rates of mass addition and heat transfer also cause numerical instability and cannot be simulated. For the current study, the vaporization rate was chosen such that the numerical scheme is stable. As a result, only low vaporization rates could be simulated. This is an issue that needs to be addressed in the future using a spatially evolving flow since high vaporization rates can cause marked changes that may not be observed in the present study.

Figure 6a shows the evolution of the kinetic energy spectrum with time after droplet vaporization is turned on. Initially, there is a rapid concentration of energy in the small scales and the corresponding increase in dissipation can also be seen in the dissipation spectrum shown in Figure 6b. However, as vaporization continues both the energy and dissipation spectra relaxes towards the spectra without any droplets. This suggests that an equilibrium state can be reached if mass addition and heat transfer rates are very low as is the present case.

Figure 7 shows the vorticity contours and product mass-fraction contours at two different time instants. Here, the droplets vaporize and in gaseous phase react with the surrounding oxidizer at infinite rate to form the product. The product mass fraction distribution is an outcome of complex droplet-fluid, scalar-velocity and droplet-scalar interactions. The product mass fraction reflects the preferential concentration of the droplets (as discussed in the earlier section) and the processes associated with transport of scalars.

LES of two-phase isotropic turbulence

LES of isotropic turbulence simulated using DNS has been carried out using a dynamic subgrid kinetic energy equation for momentum closures.

Figure 8a compares the kinetic energy spectra obtained for both coupled and un-coupled (un-filtered) DNS and LES. For uncoupled case (ϕ=0) LES captures the DNS spectra over all the resolved wavenumbers. At high wavenumbers there is sharp drop off in the LES spectra. However, some of the unresolved energy appears as k_{sgs} as shown in Figure 8b.

The exact interpretation of the energy resolved by the LES and modeled by the subgrid kinetic energy is difficult in spectral space since the present physical space LES uses a box filter and LES cut-off wavenumber does not exactly match the spectral cut-off. Hence, k_{sgs} also contains some of the resolved scale energy and therefore, it is difficult to differentiate between the unresolved and resolved scale contribution to k_{sgs}.

For the momentum-coupled case, DNS shows an increase in kinetic energy at the high wavenumbers. Although this trend is captured by the LES there is some discrepancy in the magnitude. In light of the above differences between the spectral and LES cut-offs, increased values of k_{sgs} (Figure 8b) at the high wavenumber would suggest that this feature is captured in LES through the subgrid model. Note that for direct comparison, both E(k) and K_{sgs} are scaled by the average kinetic energy ($1/2q^2$).

Figure 9a shows the LES result and by comparing it to Figure 3a, one can see that the dissipation of energy with increasing mass loading is accurately captured. However, the magnitudes are not in very good agreement and is attributed to the fact that the unresolved energy (k_{sgs}) is not included in the calculations. Similar to Fig. 3b, Fig. 9a illustrates the variation of dissipation skewness with mass loading. Since, dissipation skewness is primarily a small-scale feature, it does no surprise that the magnitude is underpredicted in the absence of small-scale energy.

The vaporization cases have also been studied with and without the subgrid model (LEM) for the species closure. Since the vaporization is very low, droplets size does not vary much and do not fall below the cut-off diameter. Thus, all the droplets are tracked using the Lagrangian tracking scheme and the terms S1 and S2 in Eq. (18) are zero. As a consequence, the void fraction in the subgrid implementation is zero. However, the key difference between the classical LES and the new subgrid based LES is that all the scalar information is carried in the subgrid and scalar transport across LES cell faces is by the splicing method (described earlier). In the current simulations since the subgrid turbulence is low, one does not expect to see drastic differences between the two approaches. Figure 10 reflects this fact and shows no observable differences between the two LES approaches. As in the momentum-coupled case there is an increase in the k_{sgs} to account for the reduced resolved kinetic energy in the LES.

To determine the impact of varying the exponent p in Eq. 15, LES with p = 4/3 (corresponding to -5/3 inertial scaling law) and p = 1 (corresponding to -2 inertial scaling law) were compared. No observable differences were seen. However, this may be an artifact of the present low vaporization case and needs to be addressed in more details using spatially evolving shear layers with realistic vaporization.

Finally, to characterize the particle energy in both DNS and LES, Lagrangian autocorrelation coefficient of the particle velocities are calculated. The autocorrelation coefficient is computed using the following relation:

$$R_{Lp,i} = \frac{\langle v_i(t_o)v_i(t_o+\tau)\rangle}{[\langle v_i^2(t_o)\rangle]^{1/2}[\langle v_i^2(t_o+\tau)\rangle]^{1/2}}$$

In the momentum-coupled case since the flow is stationary, t_0 can be arbitrarily chosen. For the vaporization case it is chosen as the time when evaporation is turned on. Figure 11a shows the autocorrelation coefficient for LES and DNS for the momentum-coupled case where as for the vaporization case (Figure 11b) a much better agreement is observed. This observation needs to be investigated further.

CONCLUSIONS

DNS using the current finite-difference code was able to capture most of the features observed in experiments and past calculations using psuedo-spectral codes. LES in the current implementation was also able to capture most of the physics (especially at the low wavenumbers) as predicted by DNS. The current LES

were restricted to low vaporization rates and to relatively low Re. However, within this limitation, results show that the present LES can deal with the changes in turbulence at the small scales. In particular, the subgrid kinetic energy model shows an ability to account for the increase in the unresolved energy. For further evaluation of the coupling between droplet motion and turbulence, spatially evolving shear layers are being simulated. Realistic vaporization rates and chemical kinetics will be simulated in these flows. Results of these studies will be reported in the future.

ACKNOWLEDGMENTS

This work was supported in part by the Army Research Office Multidisciplinary University Research Initiative grant DAAH04-96-1-0008. Computations were carried out under the DoD HPC Grand Challenge Project at ARC, Huntsville. The authors would like to acknowledge Dr. P. K. Yeung at Georgia Tech for the stochastic forcing scheme and V. K. Chakravarthy for the zero-Mach number code.

REFERENCES

Boivin, M., Simonin, O. and Squires, K. D. (1998) "Direct Numerical Simulation of Turbulence Modulation by Particles in Isotropic Turbulence," J. Fluid Mech., Vol. 375, pp. 235-263.

Calhoon, W.H. and Menon, S. (1996) "Subgrid Modeling for Reacting Large-Eddy Simulations," AIAA 96-0516, 34th AIAA Aerospace Sciences Meeting.

Calhoon, W.H. and Menon, S. (1997) "Linear-Eddy Subgrid Model for Reacting Large-Eddy Simulations: Heat Release Effects," AIAA 97-0368, 35th AIAA Aerospace Sciences Meeting.

Chakravarthy, V. K. and Menon, S. (1997) "Characteristics of a Subgrid Model for Turbulent Premixed Combustion," AIAA Paper No. 97-3331, 33rd AIAA/ASME/SAE/ASEE Joint Propulsion Conference and Exhibit, Seattle, Wa, July 6-9.

Chen, X.-Q. and Pereira, J. C. F. (1998) "Computation of Particle-Laden Turbulent Gas Flows Using Two Dispersion Models," AIAA Journal, Vol. 36, No. 4, pp. 539-546.

Chen, K-H. and Shuen, J.-S. (1993) "A Coupled Multi-Block Solution Procedure for Spray Combustion in Complex Geometries," AIAA 93-0108, 31st AIAA Aerospace Sciences Meeting, Reno, NV.

Faeth, G. M. (1983) "Evaporation and Combustion of Sprays," Progress in Energy and Combustion Science, Vol. 9, pp. 1-76.

Elgobashi, S. E. and Truesdell, G. C. (1992) "Direct Simulation of Particle Dispersion in a Decaying Isotropic Turbulence," Journal of Fluid Mechanics, Vol. 242, 655-700.

Elgobashi, S. E. and Truesdell, G. C. (1993) "On the Two-way Interaction Between Homogeneous and Dispersed Solid Particles. I: Turbulence Modification," Phys. Fluids A, Vol. 5 (7), 1790-1801.

Elgobashi, S. E. and Truesdell, G. C. (1994) "On the Two-way Interaction Between Homogeneous and Dispersed Solid Particles. II: Particle Dispersion," Phys. Fluids A, Vol. 6 (3), 1405-1407.

Eswaran, V. and Pope, S. B. (1988) "An Examination of Forcing in Direct Numerical Simulations of Turbulence," Computers and Fluids, Vol. 16, No. 3, pp. 257-278, 1998.

Kerr, R. M. (1985) "Higher-order Derivative Correlations and the Alignment of Small-scale Structures in Isotropic Numerical Turbulence," J. Fluid Mech, V 153, pp. 31-58.

Kerstein, A. R. (1989) "Linear-Eddy Model of Turbulent Transport II. Application to Shear Layer Mixing," Combustion and Flame, Vol. 75, pp. 397-413.

Kerstein, A. R. (1991) "Linear-eddy Modelling of Turbulent Transport. Part 6. Microstructure of Diffusive Scalar Mixing Fields," J. Fluid Mech, V 231, pp. 361-394.

Kerstein, A. R. (1992) "Linear-Eddy Model of Turbulent Transport 4. Structure of Diffusion-Flames," Comb. Sci. and Tech., Vol. 81, pp.75-96.

Kim, W.-W. and Menon, S. (1999) "Large Eddy Simulation of a Gas Turbine Combustor Flow," Combustion Science and Technology (to appear).

Lazaro, B. J., and Lasheras, J. C. (1992) "Particle Dispersion in the Developing Free Shear Layer. Part 2. Forced Case," J. Fluid Mech., Vol. 235, pp. 179-221.

Martin, J. E. and Meiburg, E. (1994) "The Accumulation and Dispersion of Heavy Particles in Forced Two-dimensional Mixing Layers. I. The Fundamental and Subharmonic Cases," Phys. Fluids, Vol. 6 (3), pp. 1116-1132.

Mashayek F. (1998) "Droplet-Turbulence Interactions in Low-Mach-Number Homogeneous Shear Two-Phase Flows," Journal of Fluid Mechanics, Vol. 367, 163-203.

Menon, S., McMurtry, P., and Kerstein, A.R. (1993a) "A Linear Eddy Mixing Model for LES of Turbulent Combustion," in Large-Eddy Simulations of Complex Engineering and Geophysical Flows, (B. Galperin and S.A. Orszag, Eds.), Cambridge Univ. Press, pp. 278-315.

Menon, S. and Chakravarthy, V. K. (1996) "Large-Eddy Simulations of Premixed Flames in Couette Flow," AIAA 96-3077, 32nd AIAA/ASME/SAE/-ASEE Joint Prop. Conference.

Menon, S. and Kim, W.-W. (1996) "High Reynolds Number Flow Simulations using the Localized Dynamic Subgrid-Scale Model," AIAA 96-0425, 34th AIAA Aerospace Sciences Meeting.

Menon, S. and Calhoon, W. (1996) "Subgrid Mixing and Molecular Transport Modeling for Large-Eddy Simulations of Turbulent Reacting Flows," Symp. (International) on Combustion, 26.

Menon, S. and Pannala, S. (1997) "Subgrid Modeling of Unsteady Two-Phase Turbulent Flows," AIAA Paper No. 97-3113, 33rd AIAA/ASME/SAE/ASEE Joint Propulsion Conference and Exhibit, Seattle, WA.

Menon, S. and Pannala, S. (1998) "Subgrid Combustion Simulation of Reacting Two-phase Shear Layers," AIAA Paper No. 98-3318, 34th AIAA/ASME/SAE/ASEE Joint Propulsion Conference and Exhibit.

Menon, S., Pannala, S., Kim, W.-W, Chakravarthy, V. K. and Henry, W. (1999) "Large-Eddy Simulations of Turbulent Fuel Sprays," DoD HPC Modernization Program Conference, Monterey, CA.

Metcalfe, R. W., Orszag, S. A., Brachet, M. E., Menon, S., and Riley, J. J. (1987) "Secondary Instability of a Temporally Growing Mixing Layer," J. Fluid Mech., Vol. 184, pp. 207-243.

Mostafa, A. A. and Mongia, H. C. (1983) "On the Modeling of Turbulent Evaporating Sprays: Eulerian versus Lagrangian Approach," Int. J. of Heat Mass Transfer, Vol. 30, pp. 2583-2593.

Oefelein, J. C. and Yang, V. (1996) "Analysis of Transcritical Spray Phenomena in Turbulent Mixing Layers," AIAA 96-0085, 34th AIAA Aerospace Sciences Meeting, Reno, NV, Jan. 15-18.

Pannala, S. and Menon, S. (1998) "Large Eddy Simulations of Two-Phase Turbulent Flows," AIAA 98-0163, 36th AIAA Aerospace Sciences Meeting.

Poinsot, T. (1996) "Using Direct Numerical Simulations to Understand Premixed Turbulent Combustion," 26th Symp. (Intn.) on Combustion, pp. 219-232.

Squires, K. D., and Eaton, J. K. (1990) "Particle Response and Turbulence Modification in Isotropic Turbulence," Phys. Fluids A, Vol. 2 (7), 1191-1203.

Squires, K. D., and Eaton, J. K. (1991) "Measurements of Particle Dispersion Obtained from Direct Numerical Simulations of Isotropic Turbulence," Journal of Fluid Mechanics, Vol. 226, 1-35.

Yeung, P. K. and Pope, S. B. (1989) "Lagrangian Statistics from Direct Numerical Simulations of Isotropic Turbulence," J. Fluid Mechanics, Vol. 207, pp. 531-586.

Yeung, P. K. (1996) "Multi-scalar Triadic Interactions in Differential Diffusion with and without Mean Scalar Gradients," J. Fluid Mech., Vol. 321, pp. 235-278.

Wang, Q. and Squires, K. D. (1996) "Large Eddy Simulation of Particle Laden Turbulent Channel Flow," Phys. Fluids, 8(5), pp1207-1223.

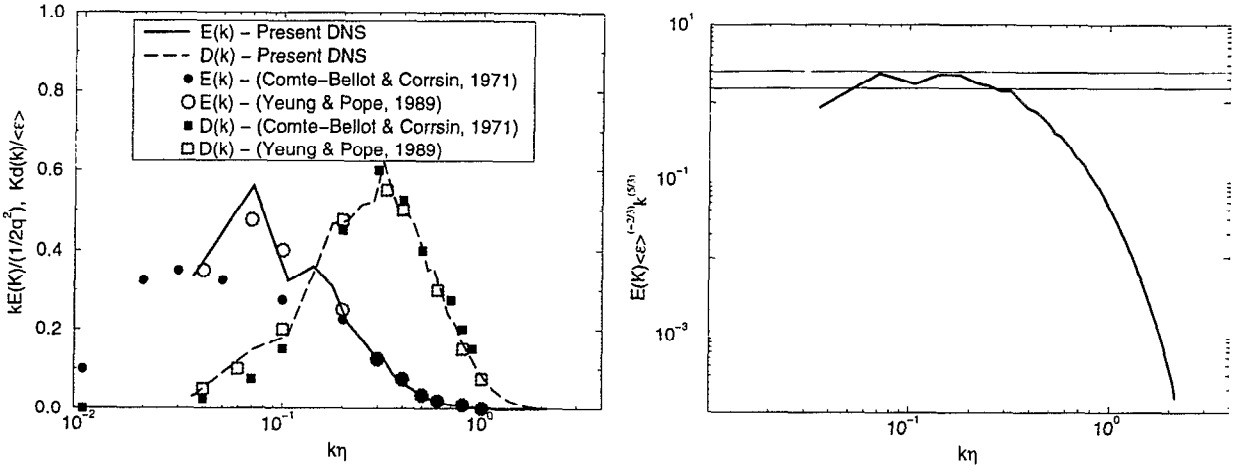

Figure 1. DNS validation. (a) Normalized kinetic energy and dissipation spectra and (b) Prediction of Kolmogorov constant.

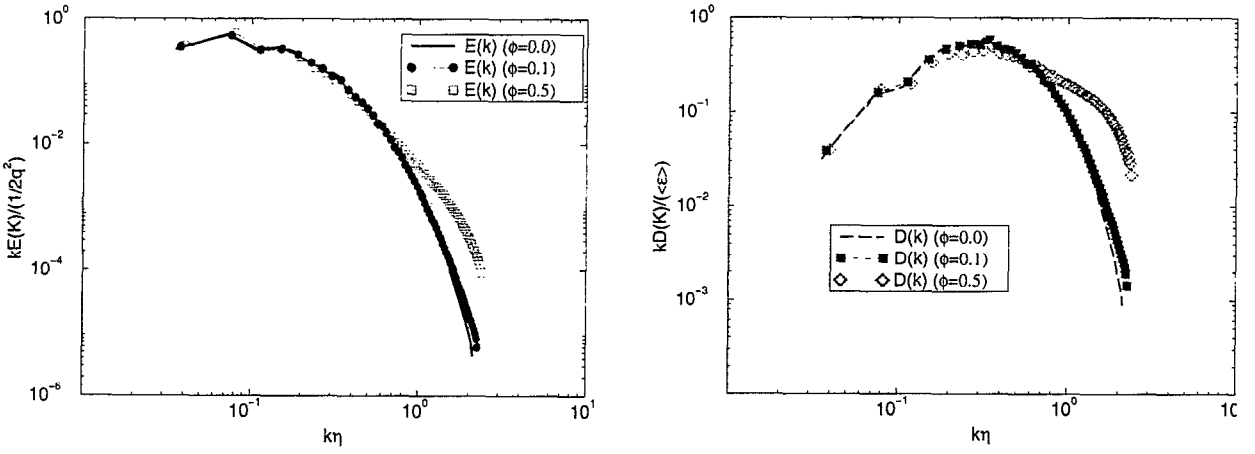

Figure 2. Effect of two-way momentum coupling with mass-loading of the droplets (a) Kinetic energy spectrum and (b) Dissipation spectrum.

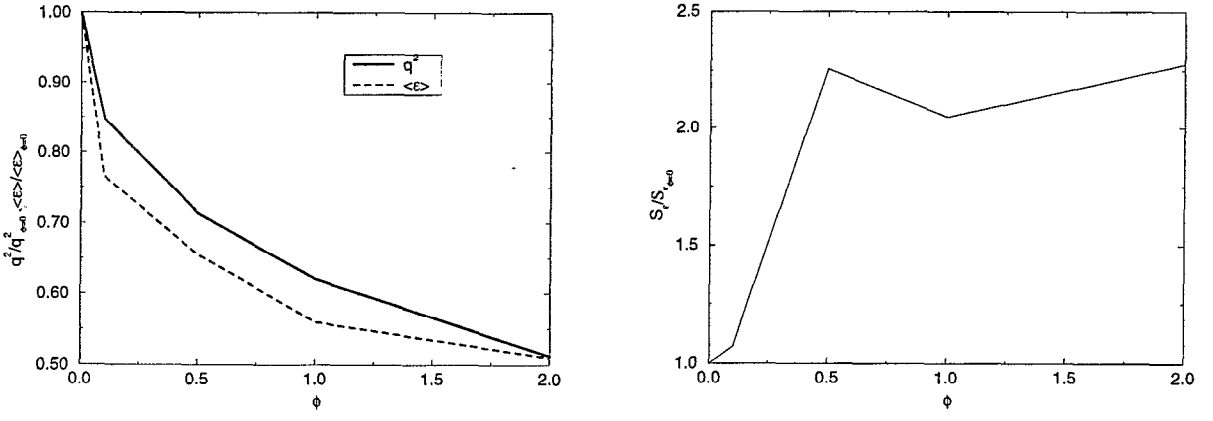

Figure 3. Variation of gas-phase properties with mass loading. a) Total kinetic energy and dissipation rate and b) Dissipation skewness.

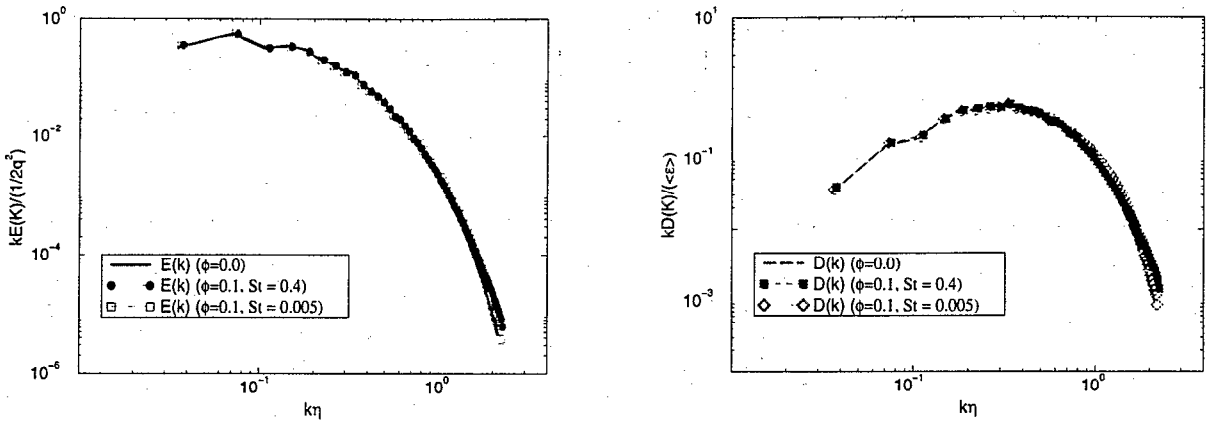

Figure 4. Effect of two-way momentum coupling with Stokes number of the droplets (a) Kinetic energy spectrum and (b) Dissipation spectrum.

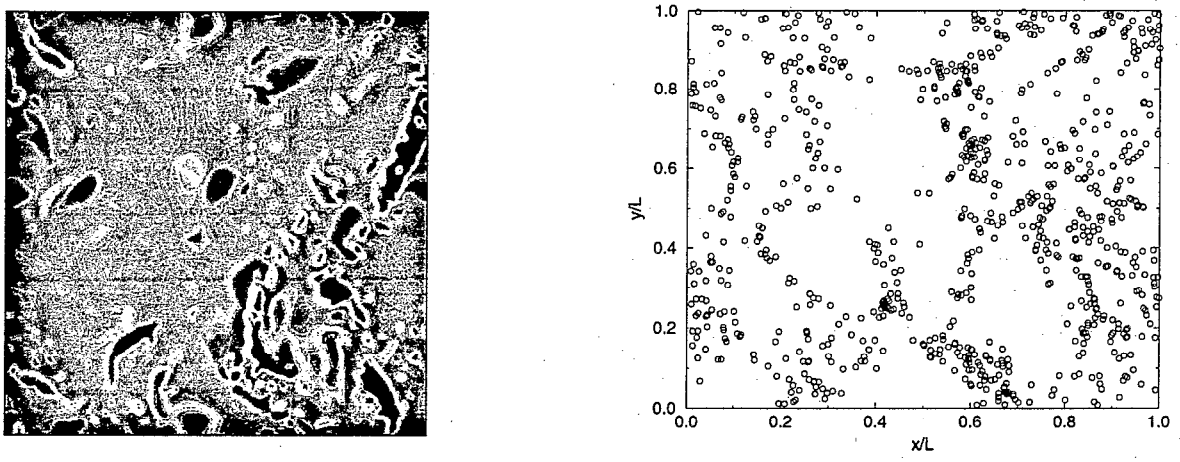

Figure 5. Preferential concentration of droplets in low-vorticity region (St = 0.4). a) Spanwise vorticity and b) Spatial distribution of droplets in the spanwise direction.

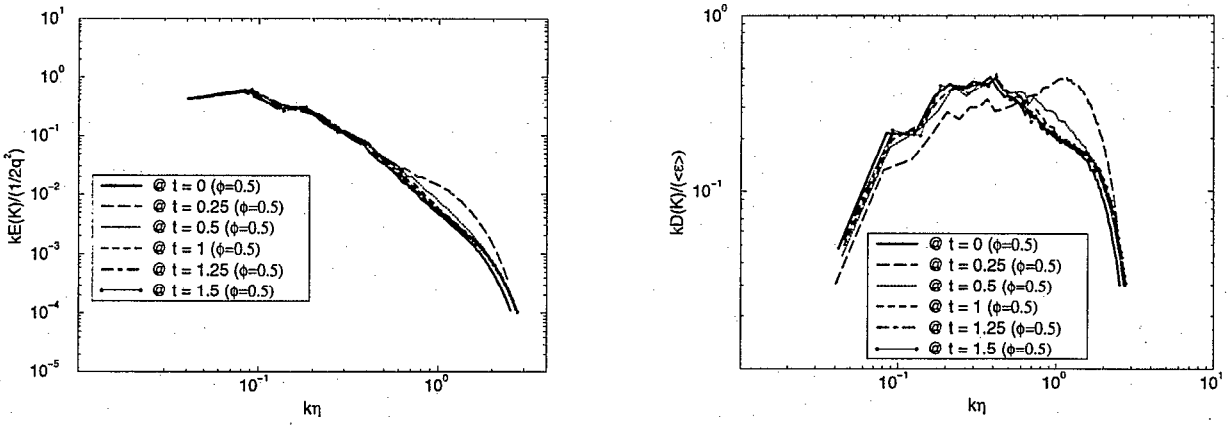

Figure 6. Time variation of effect of two-way coupling with vaporizing droplets (a) Kinetic energy spectrum and (b) Dissipation spectrum.

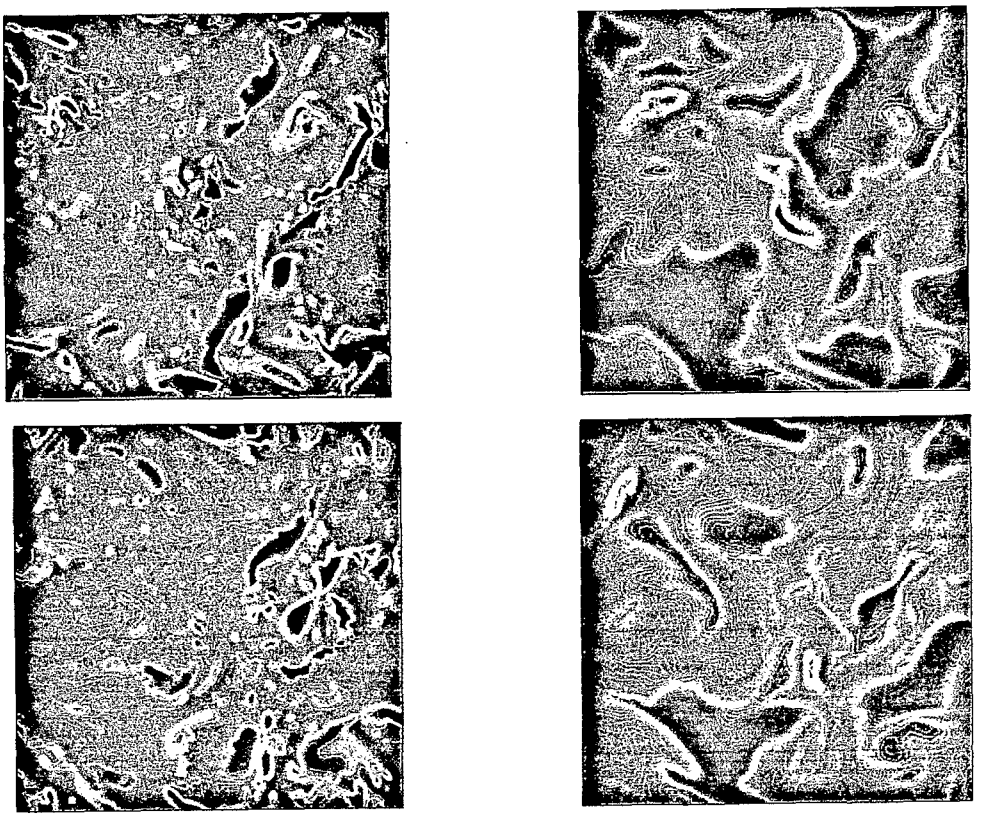

Figure 7. Snapshots of span-wise vorticity (left) and product-mass fraction distribution (right) at two different time instants for St=0.4 and ϕ=0.5.

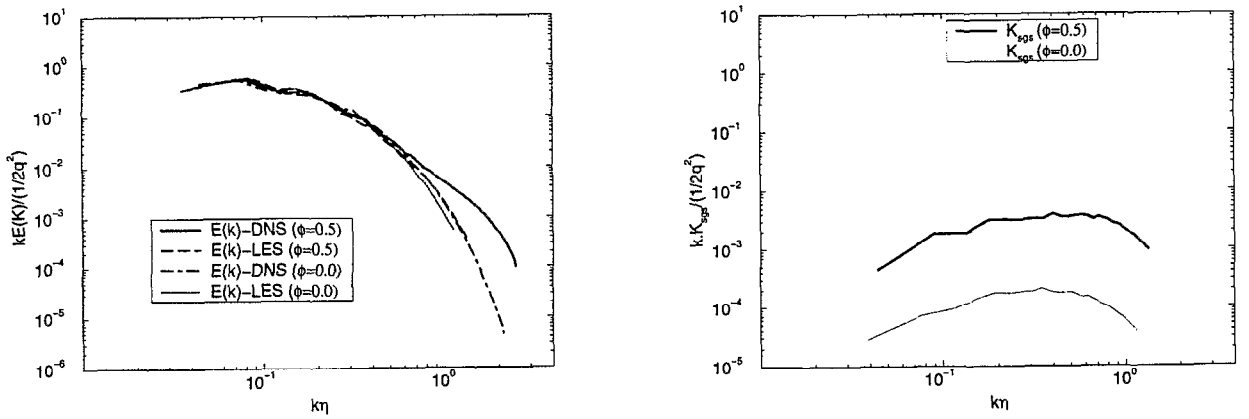

Figure 8. Comparison of LES with DNS for two-way momentum coupling for St=0.4 (a) Kinetic energy spectrum and (b) Subgrid kinetic energy spectrum.

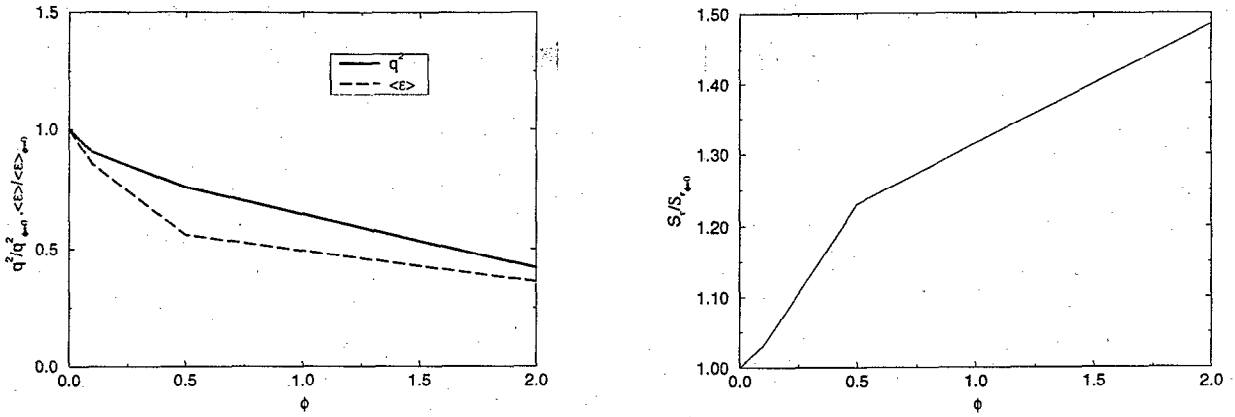

Figure 9. Variation of gas-phase properties with mass loading as predicted by LES. a) Resolved total kinetic energy and dissipation rate and b) Dissipation skewness computed using resolved scale field.

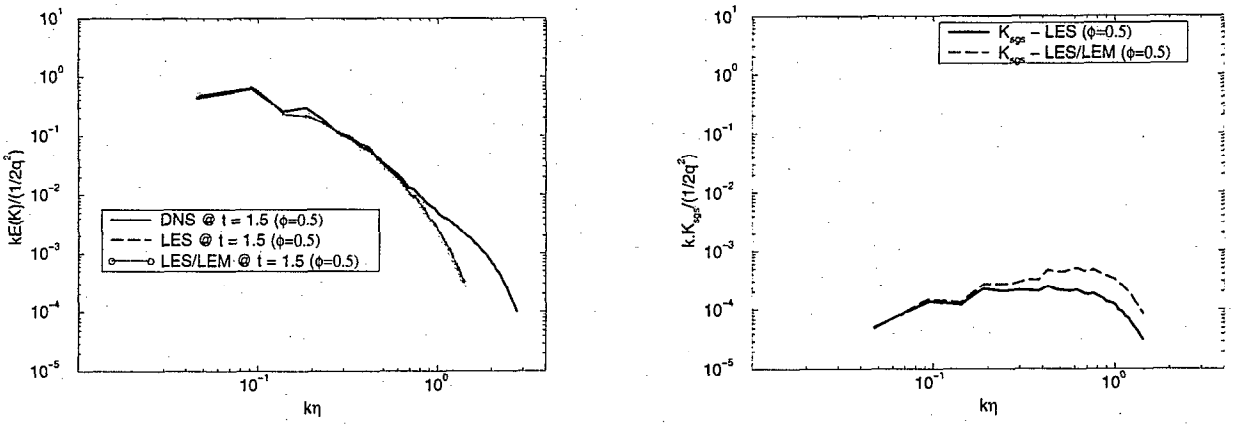

Figure 10. Comparison of LES with DNS for two-way coupling for vaporizing droplets of St=0.4 (a) Kinetic energy spectrum and (b) Subgrid kinetic energy spectrum.

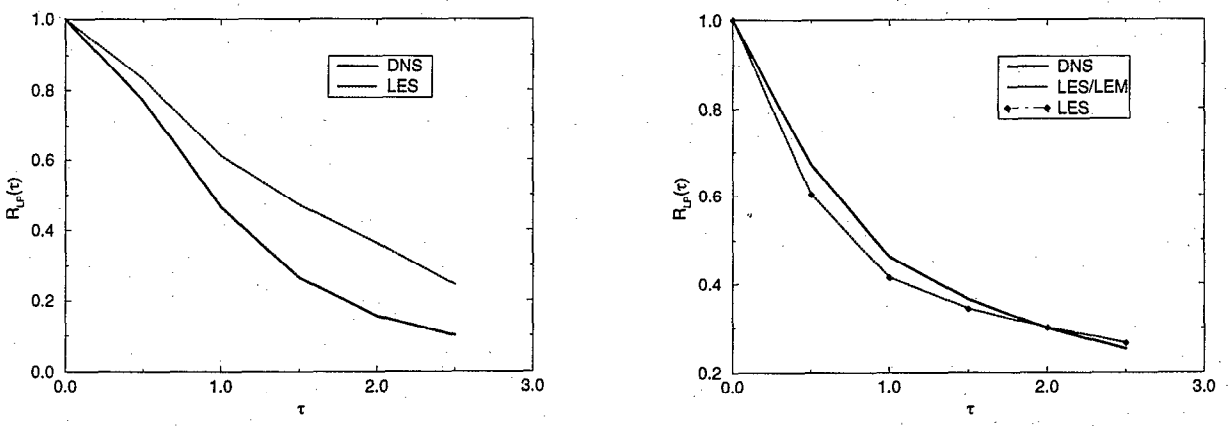

Figure 11. Time evolution of fluid-particle correlations for St=0.4 and ϕ=0.5. (a) Momentum coupling and (b) Two-way coupling with vaporizing droplets.